ACS APPLIED MATERIALS & INTERFACES

Article

Antifungal nanocomposites inspired by titanate nanotubes for complete inactivation of Botrytis cinerea isolated from tomato infection.

Vicente Rodríguez-González, Ruth B. Domínguez-Espíndola, Sergio Casas-Flores, Olga A. Patrón-Soberano, Roberto Camposeco Solis, and Soo Wohn Lee

ACS Appl. Mater. Interfaces, **Just Accepted Manuscript** • DOI: 10.1021/acsami.6b10060 • Publication Date (Web): 26 Oct 2016

ACS Publications

ACS Applied Materials & Interfaces is published by the American Chemical Society. 1155 Sixteenth Street N.W., Washington, DC 20036

Antifungal Nanocomposites Inspired by Titanate Nanotubes for Complete Inactivation of *Botrytis cinerea* Isolated from Tomato Infection.

V. Rodríguez-González,[1] R. B. Domínguez-Espíndola,[2] S. Casas-Flores,[3] O. A. Patrón-Soberano[3], R. Camposeco-Solis[1] and S-W. Lee[4]*

1. División de Materiales Avanzados, Instituto Potosino de Investigación Científica y Tecnológica, Camino a la Presa San José 2055, Col. Lomas 4a. sección, C.P. 78216 San Luis Potosí, S.L.P., México. E-mail: vicente.rdz@ipicyt.edu.mx

2. Posgrado en Ingeniería y Ciencias Aplicadas. Universidad Autónoma del Estado de Morelos. Av. Universidad # 1001, Col. Chamilpa, Cuernavaca, Morelos C.P. 62209, México

3. División de Biología Molecular, Instituto Potosino de Investigación Científica y Tecnológica, Camino a la Presa San José 2055, Col. Lomas 4a. sección, C.P. 78216 San Luis Potosí, S.L.P., México.

4. Global Research Laboratory, Sun Moon University, Galsan-Ri, Tangjung-Myon, Asan Chungnam 336-708, South Korea.

*Corresponding Author: V. Rodríguez-González, Ph.D.

E-mail: vicente.rdz@ipicyt.edu.mx, vicenrg@hotmail.com

ABSTRACT

Antifungal silver nanocomposites inspired by titanate nanotubes (AgTNTs) were successfully evaluated for the effective inactivation of the phytopathogenic fungus *Botrytis Cinerea* within 20 minutes. One dimensional $H_2Ti_3O_7$ nanotubes functionalized with silver nanoparticles (AgNPs) exhibit unique surface and antifungal properties for the photoinactivation of *B. Cinerea.* Nanostructured titanates were synthesized by the eco-friendly, practical, microwave-induced, hydrothermal method followed by a highly monodispersive AgNP UV-photodeposition. Protonated nanotubes of ~11 nm in diameter and four-layers displayed high surface areas, 300 m^2/g, with a size functionalization of 5 nm for the AgNPs. UV-vis DRS and XPS allowed the characterization and/or quantification of surface reactive species and cytotoxic silver species such as Ag°, Ag^+.

The effective biocidal properties of the nanocomposites were confirmed by using the well-known gram-negative bacteria *Escherichia coli*, and then proceeding to the effective inactivation of the phytopathogenic fungus under visible light. The photoassisted inactivation mechanism was examined by HAADF-STEM, HRTEM and FESEM electronic microscopies. A plasmalemma invagination due to oxidative stress caused by reactive oxygen, silver cytotoxicity species and AgTNT sharp morphology damage expands the conidia to induce the cell death. The impact of the eco-friendly inactivation is significant because of the ease to be carried out and the possibility of being performed *in-situ* with plants like tomato and grapes, which are ranked among the most valuable agricultural products worldwide.

KEYWORDS: *Botrytis Cinerea;* titanate nanotubes, *E. coli,* phytopathogenic, invagination, AgNPs, antifungal, vacuolation,

Introduction

Plant diseases have been studied because of the economic production constraints associated with pathogenic microorganisms.[1] Early recognition of plant diseases dates from 330 B.C. Fungi and bacteria are mainly responsible for plant diseases worldwide. Substantial attacks by microorganisms occur not only during the harvest, but also during post-harvest steps. *Botrytis cinerea* is one of the most important sclerotial plant pathogens in agriculture. This fungus has been identified as a pathogen of more than 235 plant species including grapes, lettuce, strawberries, tobacco and tomato, producing a grey powdery mycotoxin mould on the infected plants.[2] *B. cinerea* is a necrotic fungus that attacks damaged parts of the plant before spreading to healthy tissue.[1-3] The infection depends on a complex sequence of biological events involving host and environmental conditions, chemical and physical interactions between the fungal propagules, and microbial interactions on the plant surface.[3-5] *B. cinerea* shows resistance to conventional fungicides and some active harmful agents remain, i.e., in the tomato body or grapes, affecting the consumer's health.[1-6] The actual cost of fungicides is estimated to be of the order of US$ 6 billion annually.[1]

Different alternative strategies have been investigated for inactivation of plant pathogenic microorganism: UV light treatment, chlorination, hydrochlorination, peroxide oxidation, and strong oxidizing disinfectants such as ozone and chloride dioxide, among others.[7-12] New strategies using nanocomposites activated with UV and visible light, which might work at room temperature, have emerged with the aim of constraining the detrimental fungicide effects on fruit and vegetable values, water and soil pollution or generation of organic matter.[13-15] The direct contact between nanoparticles and the fungal cell wall is necessary to induce cell damage during the photocatalytic inactivation, where the damage of the cytoplasmic membrane could be the

main killing mechanism that has been reported.[13-17] On the other hand, the generation of reactive oxygen species (ROS) under UV-visible illumination is helpful for the photoactive properties. The hydroxyl radical (OH), which is generated on the surface of an illuminated semiconductor, usually titanium dioxide (TiO_2), plays a key role, but some other morphological proprieties and reactive sites could be involved in enhancing the oxidative stress on the pathogenic fungus.[14-15, 17-18]

The antimicrobial nanomaterials should be physically and chemically stable in aqueous environments where most of the pathogenic microorganisms undergo a reproduction process and pathogenesis; this means that the nanomaterials should not be irreversibly aggregated during the inactivation process, and remain chemically stable to photocorrosion. Besides, the ideal nanocomposite must also exhibit wide antimicrobial activity at ambient temperature in a very short time in order to inhibit damage to flora and humans from the pathogenic microorganisms or progress on antimicrobial resistance. The nanocomposite should not be toxic and it must not generate any harmful effect during or at the end of the inactivation process. Lastly, it should be a low-cost material with hydrophilic properties and stable for reuse during several cycles.[16]

Layered titanate has structural similarity to titanium dioxide, both composed of TiO_6 octahedral units connected by sharing corners and edges.[19] The corner-sharing connected TiO_6 octahedral arrangement of layered materials favors the atom doping or molecular assembly, which is more difficult to attain with more compact TiO_2 polymorphs. The spatial arrangement of the octahedral-unit-building blocks gives titanate attractive characteristics such as large ion-exchange capacity, high surface specific area, hydroxylated surface and titanate flexible layers. Its polymorphs are 1D linear and flexible structures (tubes, wires, or belts), 2D sheets and

hierarchical 3D structures. In general, their chemical formulae are $H_xTi_{2-x/4}\square_{x/4}O_4.zH_2O$ (where $\square$ denotes a vacancy, and x is close to 0.7).[19-20]

In the present study, the surface activity and structural properties of the silver nanocomposites were characterized and studied in order to obtain a deeper insight into the antifungal properties of silver protonated nanotubes that are directly correlated with the inactivation of the phytopathogenic fungus *B. cinerea*. The ratio of silver species was determined by XPS and UV-vis DRS was then correlated with antimicrobial and photocatalytic activities.

The pathway of *B. cinerea* inactivation by AgNPs functionalized on one-dimensional-protonated nanotubes under a simulated solar lamp was investigated. Firstly, the biocide properties of the nanocomposites were verified by using as a model the gram-negative bacteria *Escherichia coli*,[21] and then proceeding with a concise discussion of the effective inactivation of the phytopathogenic fungus *B. Cinerea* by means of electronic microscopies (FESEM, HRTEM and STEM-HADFF) correlated with spectroscopic physicochemical characterization of the inorganic nanomaterials, following the conidial evolution during the photocatalytic inactivation under visible-light irradiation.

Materials and Methods

Synthesis and silver functionalization of titanate nanotubes

$H_2Ti_3O_7.(OH_2)$ nanotubes were successfully synthesized by a practical one-step hydrothermal method in a microwave reactor (Eyela MWO-1000 Wave Magic) following a previous procedure (Hy-MWM).[22] The cylinder-like titanate nanotubes were attained in 4 h under continuous microwave irradiation of maximum 195 W (2450±30 MHz) and alkaline conditions at 150°C in 100 mL of a 10 M NaOH aqueous solution stirred at 500

rpm. Afterwards, the obtained material was cooled to room temperature and neutralized with 5 N HCl. Then, the resulting powder was washed thoroughly with distilled water until the pH of the washing solution was~7. The powder was filtered using a hydrophilic polypropylene filter (Pall, 0.2 μm) in a vacuum system and dried at 95°C for 12 h.

Photo-assisted functionalization with silver nanoparticles

The photoassisted functionalization of silver nanoparticles was performed over titanate nanotubes and a commercial titanium dioxide, the P25 Degussa material (75% anatase, and 25% rutile) used as bare material. The photodeposition of Ag_xO_y nanoparticles was carried out as follows: an ethanol solution of $AgNO_3$, keeping three loadings (0.5, 1 and 3 wt. %) in order to define the optimal biocide properties of the AgNPs, and the appropriate amount of TNTs previously prepared by Hy-MWM, were placed in a small glass reactor. The suspension was placed under vigorous stirring for 5 min and then in ultrasonic bath for 5 min to ensure the complete disaggregation of agglomerated particles. Afterwards, the slurry was maintained under magnetic stirring at 500 rpm for 1 h and, at the same time, irradiated with a 17 W UVC lamp (TecnoLite G15T8, 254 nm, 1168 $\mu W/cm^2$). Then, the suspension was filtered using a hydrophilic polypropylene filter (Pall, 0.2 μm) in a vacuum system. The solids were completely dried overnight in an oven at 80 °C.

The prepared silver titanate nanotubes were identified as TNTsXAg, where X denotes different silver contents in wt. %.

Surface characterization of silver functionalized nanotubes (TNTsAg)

The silver functionalized nanotubes (TNTsAg) were characterized by high resolution transmission electron microscopy. HRTEM images were obtained with a FEI Tecnai F30 microscope equipped with a tungsten field emission gun operated at 300 keV. High-angle

annular dark field (HAADF) imaging was performed in a scanning transmission electron microscope (STEM) and a field emission scanning electron microscope (FE-SEM) was applied to study the TNT morphology and silver dispersion by means of a Helios NanoLab 600i equipped with an Advanced Dual Beam for ultra-high resolution imaging. The elemental composition of the samples was determined by energy dispersive X-ray spectroscopy (EDS) with an EDAX spectrometer fitted to the TEM. The powdered samples were ultrasonically dispersed in isopropyl alcohol and supported on holey carbon coated copper grids. Particle size and nanotube diameter distribution histograms for the samples were established from the measurements of 200–300 particles. The average particle diameter was calculated by using the following formula: $ds = \dot{}\Sigma nidi/\dot{}\Sigma n$i, where *ni* is the number of particles of diameter *di*. UV-vis RDS spectra and band gap energy data were obtained using a spectrophotometer UV-Vis-NIR Agilent Technologies model Cary 5000 Series with an integration sphere. XPS was performed with a XPS, Multiab 2000 system with an X-ray AlKα (1486.6 eV) source operated at 15 Kv and 1 mA, 400W and 1 ma. The binding energy was determined by using carbon C (1 s) as reference line (284.6 eV). The spectrometer was operated at pass energy of 23.5 eV, and the base pressure in the analysis chamber was maintained in the order of 3×10^{-8} mbar. Peak fitting were done by using the XPS fitting program XPSPEAK 41 with Shirley background.

Photoassited inactivation of *Botrytis cinerea* conidia and *Escherichia coli* cells

The photocatalytic inactivation test carried out on the *B. cinerea* strain was isolated from a tomato field at San Luis Potosi, Mexico, and identified by PCR amplification of 18S rDNA using the oligonucleotides ITS1 and ITS4.[23] *B. cinerea* conidia is described as follows: All Pyrex glass apparatus and materials used in this experiment were sterilized at 121°C for 45 min in an autoclave. *B. cinerea* was routinely grown on Potate Dextrose

Broth (PDB, DifcoTM) at 28°C for 10 days. Afterwards, conidia were collected with sterilized saline water and counted in a hemocitometer. All the photocatalytic inactivation experiments were carried out in 30 mL Petri dishes (90 × 15mm) with constant magnetic stirring and irradiated with a halogen lamp (Eco cool halogen shine 30W, Yazawa Corporation) to provide solar simulated light irradiation in the presence of 30 mg of photoactive silver nanotubes. At fixed time intervals, samples were taken from the suspension, diluted and plated on PDA and LB plates for *B. cinerea* and *E. coli*, respectively, in triplicate. After 96 h of incubation at 28°C in the dark, the number of viable conidia and cells was determined as colony-forming units (CFU) corresponding to at least one surviving conidium or cell; finally, the collected cells (*B. cinerea* concentration of ~1 x10^6 CFU/mL) were diluted. The number of colonies on a sample must be approximately 70 in order to assure enumeration and reproducibility.

E. coli cells were used as a reference for the photo-inactivation viability of nanotubes based on the numerous studies reported in the literature.[13, 20, 24-26] *E. coli* was grown in a liquid Luria Bertani (LB) medium by incubating it for 16 h at 37°C. The overnight culture was centrifuged twice at 4500 rpm for 10 min, the supernatant discarded and bacterial pellets resuspended in 20 mL of a sterile saline solution. An initial *E. coli* concentration of ~1 x10^8 CFU/mL was used for all the experiments and the collected cells were diluted keeping in mind that the number of colonies on a sample must be 350. The samples were plated in triplicate on LB plates plus 1.5% bactoagar (Bioxon). After overnight incubation at 37°C, the colonies were visually identified and counted.

Morphological *B. cinerea* characterization

B. cinerea was characterized using SEM. Cell samples collected at representative time intervals during inactivation and before were placed in a pellet. The conidium pellets were fixed in 3% glutaraldehyde in a sodium phosphate buffer, 100mM, at pH 7.4 and 4 °C for 24 h; the samples were washed four times with the buffer for 15 min each time. Afterwards, the samples were post-fixed with 1% OsO_4 in buffer for 2 h at 4°C. The samples were gradually dehydrated with absolute ethanol from 30 to 100% for 10 min with each concentration, and washed twice with 100% absolute ethanol, each washing lasting 15 min. The critical point drying process was performed in a Tousimis Samdri-PVT-3D, and the dry samples were mounted in order to perform the gold sputter coating in a Cressington apparatus Model 108 auto and examined in a FEI model Quanta 200 SEM. The SEM was adjusted at 18kV, spot 5.5, and WD 10mm, taking the micrographs with an Everhart Thornley Detector (ETD).

The ultrastructure of *B. cinerea* was observed by TEM, and the conidium pellets were fixed, post-fixed and gradually dehydrated with absolute ethanol until 100% as previously described for SEM. Then, two changes with 100% propylene oxide (PPO) for 15 min each were done at RT (Room Temperature). The pre-inclusion was done in EPON 812 and PPO 1:1 in a desiccator for 48h at RT. One change of 100% EPON 812 was done in a rotating device for 4 h. The cell pellets were embedded and polymerized at 60 °C for 48 h. Ultrathin sections were obtained in an ultramicrotome (RMC) and placed in FCF -100 Cu and contrasted with 2% uranyl acetate for 15 min, followed by 2% lead citrate for 7 min. Finally, the samples were examined in a JEM-200 CX (JEOL) transmission electron microscope at 100kV and equipped with a digital camera (SIA, Germany) to record selected images and Tecnai F30 (FEI) with EDS.

Results and discussion

Physicochemical features of photoactive $H_2Ti_3O_7$ nanotubes

The thickness of the $H_2Ti_3O_7$ nanotubes was found to be ~11 nm with four layers, and a length up to 300 nm, Fig. 1a-b.[22] One-dimensional nanotubes tended to agglomerate by forming bundles, where HAADF and TEM images show the nanotubular morphology, Fig. 1a-b. All the obtained tubes featured open-end sharp structures. The development of long nanotubes may provide the high surface area that would be a great factor to tailor bactericide properties by the high monodispersion on the surface of functionalized AgNPs at different loads. In Fig. 1c, the FESEM image shows the high dispersion of AgNPs. The histogram distribution inset in Fig. 1c displays the dispersion range of AgNPs with the maximum at 5 nm for the TNTs3Ag composite. The HRTEM image clearly confirms the four-layered TNT nanotubes morphology with open ends and an interlayer distance of 0.72 nm, Fig. 1d.[19]

In Fig. 2a, the nitrogen of adsorption-desorption isotherms presents an isotherm form that agrees well with a layered mesoporous material, which is type IV with mesoporosity. The AgNP functionalization causes almost 10% of decrease in surface specific area and a decrease in pore size of 0.2 nanometres according to the data from the BJH desorption isotherm. Table 1.[27] The large narrow hysteresis type H2 from 0.2 to 1.0 of relative pressure is maintained even after the silver functionalization. however a smooth loss of surface area and a reduction in the heights of the hysteresis loops were observed. The surface area loss means that the AgNPs were incorporated all over the surface area and porosity. The small change of hysteresis loop occurs from 0.72 to 0.95 P/P_0 due to the

incorporation of AgNPs to the external surface of the nanotubes, increasing the interparticle voids, H2 type. This hysteresis also is due to the capillary condensation in the interlayer space.[28]

Table 1. The physical characteristics of the bare TNT and the AgNPs-loaded catalyst

Sample	S_{BET} (m^2/g)	D_p (Å)	E_g (eV)
TNT	326	125	3.0
TNTs0.5Ag	296	115	3.0
TNTs1Ag	294	105	3.1
TNTs3Ag	291	106	3.1

The XRD characterization shows the typical broadening of peaks due to the detrimental factors of their specific nanostructure. The observed reflections are attributed to the titanate phase nanotubes $H_2Ti_3O_7$ (JCDPS 36-0654) corresponding to TNT and TNTs3Ag composite patterns. The planes of the orthorhombic phase are labelled in Fig. 2b. The intense peak characteristic of the silver metallic phase is observed in the sample loaded with 2 wt. % of Ag (JCDPS 04-0783). It is supposed that the nanotubes are functionalized with AgNPs in nanometric size. The broadening of the peaks, notably the (001) at 10° of 2 theta, is caused by the hydroxylated surface and interlayers of the nanotubes[29] that were used by the silver ion to be anchored and grow on the titanate surface, Fig. 2b).

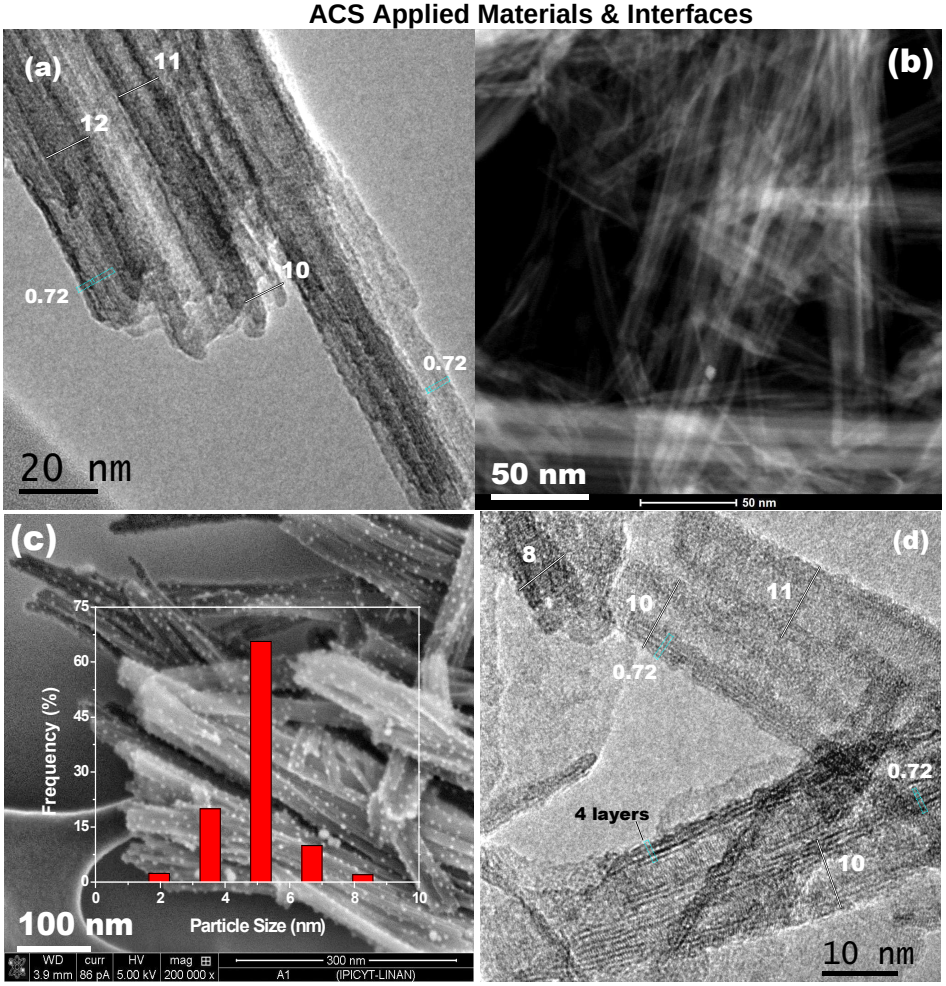

Fig.1. Selected TEM and SEM images of $H_2Ti_3O_7$ nanotubes synthesized via a hydrothermal method: a) The HRTEM image of TNTs1Ag shows the thickness of the $H_2Ti_3O_7$ tubes featuring open-end sharp structures, b) the HAADF image of TNTs1Ag shows the layered structure forming translucent bundles, c) the FESEM image of TNTs3Ag shows AgNPs highly dispersed over the nanotube surface and AgNP average particle size, and d) the four layered nanotube structure of TNTsAg1 with interlayer distance d_{100} of 0.72 nm.

UV–vis DRS and FE-SEM characterization procedures confirmed the presence of AgNPs on the surface (~5 nm) of the 1-D nanostructures (Fig. 2c), which are highly dispersed and are suitable for the fungus biocide purpose. The band-gap energies of silver titanates were 3.1 eV in average and 3.0 eV for TNTs0.5Ag, which could be excited mostly by UV irradiation. The AgNPs help the visible light absorption because AgNPs extend the Eg band gap to lower energy, Fig. 2c.[14] It is clear that at increasing the silver load a new broader band appears centered about 520 nm for TNTs1Ag and shifted to 700 in the case of TNTs3Ag. This band is

directed related to the size and proximity of AgNPs that cause absorption. The selected FESEM image of TNTs3Ag shown in Fig. 1(c) confirms the average size of 5 nm and some bigger Ag nanoparticles can be seen that may cause the broader band absorption that maybe due to Surface Plasmon Resonance (SPR) of AgNPs. The SPR effect supports the high monodispersion of silver nanoparticles on the surface of the nanotubes as it was confirmed by the EDS analysis, Fig. 2d. Lower loads of silver is challenging the observations by HRTEM; HAADF or FESEM, Fig. 1 a, b and d.

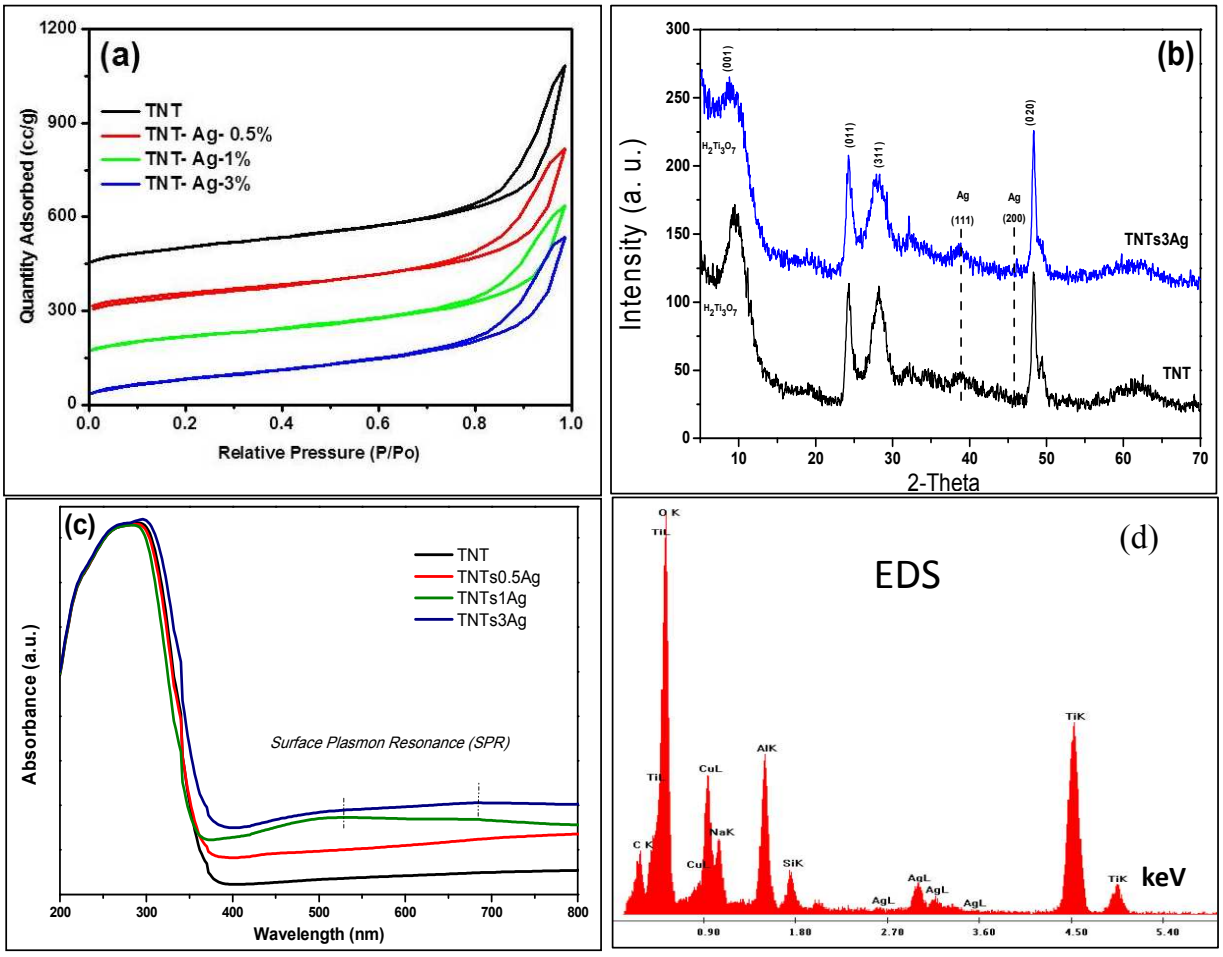

Fig.2. a) Image of adsorption-desorption N_2 isotherms for inspired silver nanotube composites, b) XRD patterns for selected layered structures, c) UV-vis DRS spectra of the nanotubes and P25, and d) EDS spectra for confirming the silver composition.

Photoassited inactivation of *B. cinerea* as a function of time

The photocatalytic activity of the nanotubes functionalized with AgNPs was evaluated first by the inactivation of *E. coli* cells, which are the most representative model of gram-negative bacteria. Fig. 3 shows the *E. coli* inactivation ratio as a function of time for the three-titanate nanotubes with different AgNP loading. The control test without catalyst showed negligible inactivation activities, suggesting that the halogen irradiation had no influence on the fatal damage of *E. coli*. Evaluation in dark conditions of the silver nanoparticles were developed to check the biocide capability of silver in absence of visible light, finding that the biocide capability for killing *E. coli* was 40% of cells in one hour. Under light irradiation, the differences in photoactivity capability of the silver titanate nanoparticles were in the following order: 3% Ag with 100% of photoinactivation followed by 1% Ag with 70% of photoinactivation and finally by using 0.5% of Ag, 60% of photoinactivation was achieved. By considering the silver loading, the photoactivation behavior, AgNPs biocide capability, sharp morphology of TNT and the achieved inactivation percent for each catalyst, the optimum catalyst was TNTs3Ag for *E. coli* photoinactivation in only 60 min. In brief, the dark conditions evaluation of the TNTs3Ag show that the difference of load of AgNPs is negligible because AgNPs have a bacteriostatic effect that mainly increases with the time of contact. The damage caused by the TNT morphology seems more serious for the *E. coli*. TNTs3Ag dark evaluation increase the bacteriostatic activity in 6.0%, but the irradiated system increases notably the killing effect because silver dispersion and its size enhance the transfer of photo-generate electrons and decrease the recombination. The obtained results show that photoactivity is the main factor for enhancing the synergic cell disruption and are in good agreement with

the literature and validate the photoactivity and biocidal properties of the synthesized silver nanotube composites.[8, 17-18, 21]

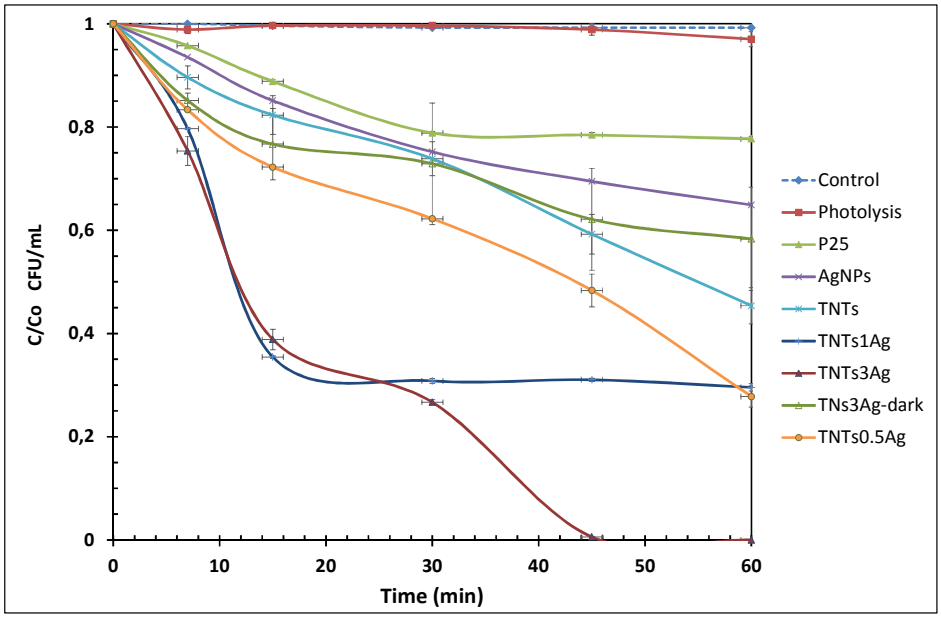

Fig.3. *E. coli* inactivation ratio as a function of time for the three photocatalysts with different AgNP contents and references

The photoassited inactivation of the *B. cinerea* fungus as a function of time is shown in Fig. 4 for the three photocatalysts and the control test. The test system without catalyst showed slight inactivation activities of almost 9%, suggesting that the halogen irradiation had tiny influence on the damage of *B. cinerea*. Dark tests of the silver titanate nanocomposites were developed to check the biocide capability of silver in absence of visible light, obtaining a biocide capability for killing B. cinerea that was 26% of cells in one hour, which is lower that the biocide capability presented for the E. coli inactivation, 36%. Under visible-light irradiation conditions for *B. cinerea*, the differences in photoactivity capability of the silver titanate nanoparticles can be observed before 30 min, where all the photocatalysts presented a photoactivity efficiency of 100%. By considering the silver

loading, photonactivation behavior, sharp morphology of TNTs, silver biocide capability and achieved inactivation percent, the optimum catalyst was TNTs0.5Ag for *B. cinerea* photoinactivation in comparison with the 1 and 3% silver loading, Fig. 5. Light irradiation had a negligible effect of about 6%. Bacteriostatic effect of AgNPs in dark conditions of the more photoactive is 14% more effective than the effect of AgNPs alone. It seems that *B. cinerea* is more sensible to the sharp morphology of TNTs achieving 78% of inhibition of the growth of the fungus. Fig. 5 confirms that by using silver titanate nanomaterials, the boosting of the photokilling effect is due to a synergic effect that helps to achieve the effective inactivation of this phytopathogenic fungus. AgNPs or TNTs did not complete the inactivation process in 60 min, but by forming the silver titanate nanocomposites their effects were of potential merit under halogen irradiation.

The total inactivation under irradiation of *B. cinerea* was achieved by TNTsAg0.5 after 20 min; with higher Ag loading, the total killing was attained after 30 min; this photokilling activity is faster than the one displayed by the TiO_2-P25 commercial reference and AgNPs from silver nitrate. Other reported methods and materials need more than one hour for the inactivation of *B. cinerea*.[11-12]

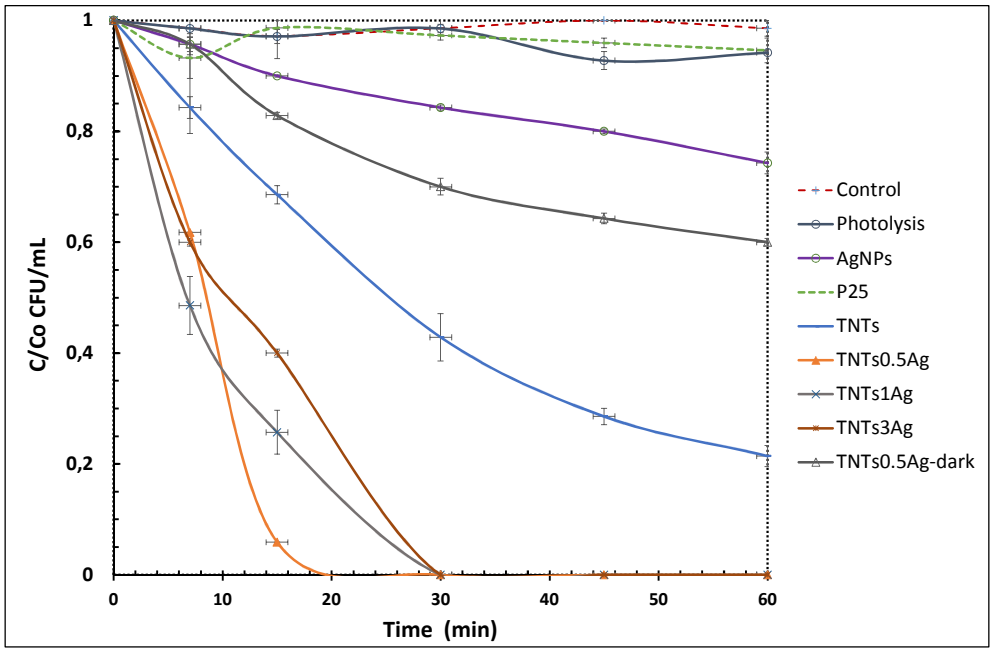

Fig.4. Photoassited inactivation of the *B. cinerea* fungus as a function of time for the three loadings of AgNPs on titanate nanotubes and controls

S. Thabet et al.[15] studied the antimicrobial effects of photocatalysis on the filamentous *B. Cinerea* by using commercial TiO_2 P25. The spores were detected after a long exposure and 77% of the cells were still cultivable after 20 h of treatment.[15] The experimental conditions, which are in contrast with our conditions, are not quite analogous, and the principal reasons for achieving the complete inactivation of *B. cinerea* in 20 min either. This fact could be related to the nanotubular morphology and synergetic silver surface species effects.

Morphology and structure of *B. cinerea*

The dimensions of the egg-shaped conidia were in the typical range of 10± 2.5 × 5±2.5 µm[12-30] with characteristic density as shown by SEM, Fig. 5a. Although there were some intact conidia, the effectiveness of the treatment was shown from the first 5 minutes; some conidia were destroyed by the photoactive silver-titanate nanotube effect under

visible light and the rest of the conidia were affected gradually. At first, the cells lost density, showing swollen vacuoles (Fig. 5b) by the time the number of dead cells was growing (Fig. 5c-d); after 45 min of interaction, all the vacuoles seemed to be empty and silver-titanate bundles were observed. Bundles agglomeration marked with white arrows can be distinguished due to the irregular morphology like fiber dense bundles in contrast to the oval transparent conidia and fungus, Fig 5d. For further approach and visualize cells in contact with titanate particles and to check their possible penetration in cells, TEM and HAADF were used.

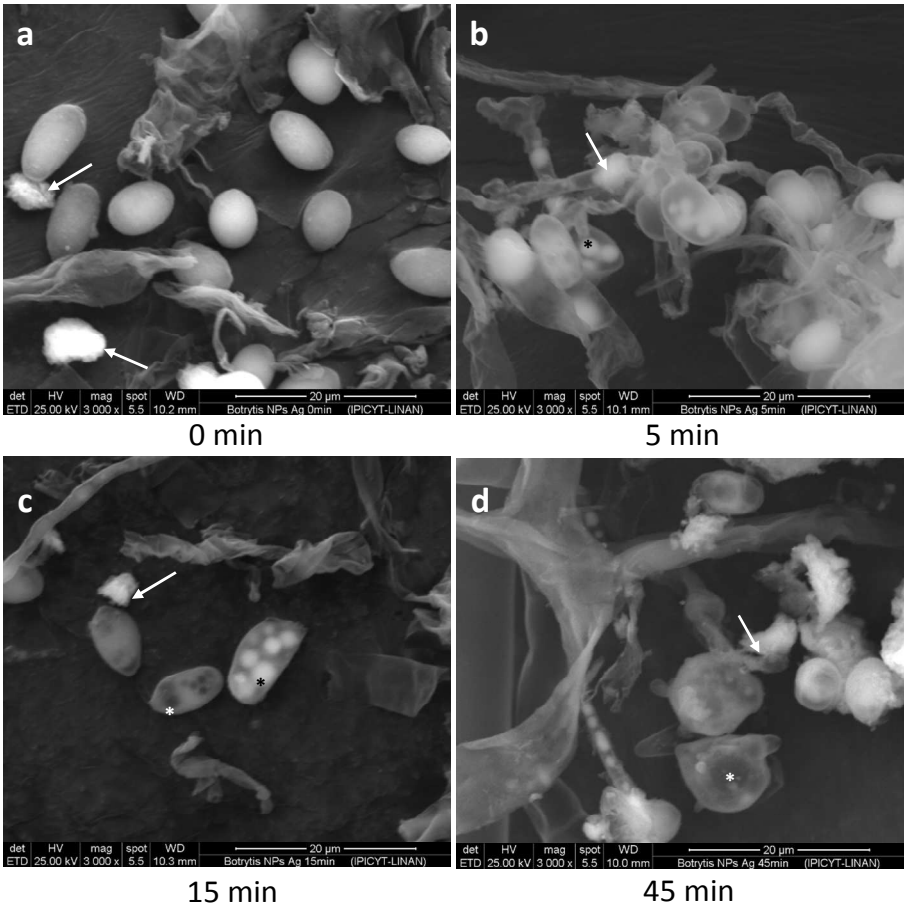

Fig.5. Selected FESEM images of the photoinactivation of the phytopathogenic fungus *B. cinerea* by silver-titanate nanotubes, TNTs1Ag at different times: a)0 min, b)5min, c)15min and d) 45min; TNTsAg bundles (white arrow), electrodense vacuole (black asterisk), and empty vacuole (white asterisk).

Direct observation of the *B. cinerea* structure

Transmission electron microscopy (TEM) was used to determine the internal structure of damaged *B. cinerea* caused by the inorganic titanate materials TNTsAg during the photocatalytic inactivation. The progressive morphological changes of *B. cinerea* are shown in the TEM images. First the conidia comprise 2-layered cell walls, a thin electron dense outer layer and a thicker electron-transparent inner one. The cell contents comprise nuclei, mitochondria and vacuoles. Plasmalemma covers the cytoplasm below the inner cell wall, all this typical characteristics of the conidia it is shown in the Fig. 6a-b where the photoinactivation process starts. In this work, it was found that some conidia have numbers of nuclei and mitochondria (Fig. 6c-d), which suggests that they are in an early germination stage.[31-33]

The TEM characterization shows only the external layer of the cell wall when the photoinactivation is complete, Fig. 6g-h. Silver-titanate deposits that are responsible of the fatal irreversible inactivation of the *B. cinerea* conidia are also observed inside the inner layer of the cell wall and on the external layer of the cell wall, Fig. 6. It is important to remark that in all the TEM images, the damages to the cells are observed and these were gradually increased until only observing the empty conidia, which agrees well with the SEM observations. The fusion of intracellular vacuoles it is observed in fig. 6 e-f, the expansion of the vacuoles is clearly observed until the cell content disappear.

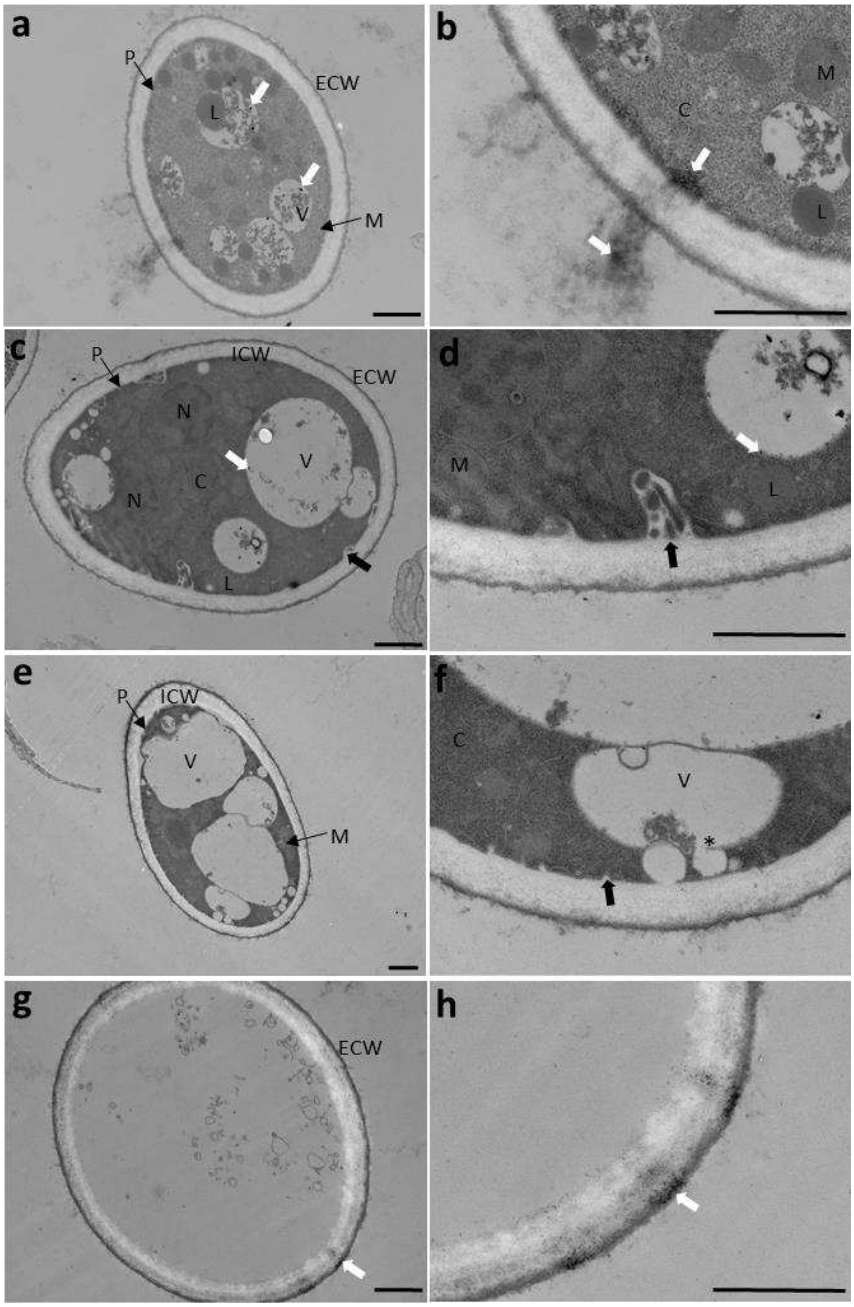

Fig. 6 Selected TEM images of the progressive morphological changes of *B. Cinerea* caused by TNTs0.5Ag photoinactivation: a) TNs0.5Ag penetration, c) vacuolation and invagination, e) vacuole fusion, g) cell death, where b, d, f, and h correspond to the magnifications of a, c, e and g, respectively. C. cytoplasm, P. plasmalemma, M. mitochondrion, N. nucleus, L. lipids, ECW, external layer of the cell wall, and ICW, inner layer of the cell wall. The bar = 1 μm.

The silver nanotubes inactivated conidia by vacuolation stemming from the damage of the external cellular wall caused by nanotube covering and penetration. Plasmalemma invagination due probably to oxidative stress caused by the ROS species (O^{2-}, HO•, •HO_2, H_2O_2, etc.) and the nanotube have open-ends that are sharp and damage the surface wall of the cell expanded the vacuole conidium cell to induce the cell viability loss. In brief, the steps observed during the photoassisted inactivation are deduced by morphological analysis since 10 to 45 minutes of interaction, in each time analyzed all steps were present, changing only the percent of degree of conidias affected: a) nanotube morphology damages the cell wall and surface cell covering with silver nanocomposites started during the adsorption time; b) when the light irradiation starts, the generation of radical species stresses the pathogenic fungus in conjunction with the AgNP bactericidal properties; ROS can also be generated during the course of normal aerobic metabolism when conidia are exposed to stress conditions.[34] The AgNPs are mainly deposited on the internal wall of the plasmalemma and vacuoles, and few nanotubes may increase the stress due to penetration and deeper damage of the cell; c), d) vacuolation and invagination start to expand the vacuoles whose damage starts with their size increase. e), f) By the time the material inside of vacuoles disappears, the irreversible destruction of the plasmalemma takes place, Fig. 6; g), h) when the annihilation of conidia is complete, only their external wall remains without any other structure. Cell disruption by oxidative stress is the main way to cause cell viability fatal loss. The difficult penetration of the cell wall by TiO_2 has already been reported in the literature.[14-13, 18] The resistance of *B. cinerea* spores to photocatalytic treatment was related to the thickness of the cell wall, which ranges from 100 to 200 nm, and also to the composition of *B. cinerea* cell wall, which is made of several complex layers of polysaccharide compounds with a thickness of 500 nm. Melanin and carotenoid compounds adsorb oxygen-free radicals and UV

light. Consequently, the presence of such pigments in *B. cinerea* cell walls could compete with composite nanoparticles in adsorbing UV radiation and trapping some reactive oxygen species generated on the catalyst surface.[15] The sharp tubular morphology seems to be the key for rapid cell loss viability by invagination.

S. Thabet el al.[15] reported the antimicrobial effects of TiO_2 on *Saccharomyces cerevisiae*, where ROS directly generated by commercial TiO_2 could then reach the cellular membrane through a locally disorganized cell wall space and cause oxidative damage. Such cells could be temporarily protected until the cell walls are sufficiently damaged due to the expressing oxidant stress response generated during photocatalytic exposure, causing loss in cell viability. In our case, the nanotube morphology and size helps to penetrate the cell to favor the intimate contact of AgNPs and ROS species with plasmalema and achieve the total inactivation of conidia in 20 min. The cell content of conidia helps the diffusion of the nanotubes among conidia.

In order to verify the presence of silver-titanate in and or on conidia, material images were acquired in STEM mode using a high angle annular dark field (HAADF) detector to distinguish between heavy and light atoms, complemented with EDS analysis (Fig. 7). The presence of AgNPs dispersed all over the conidia were identified only as silver maybe because the quantity of titanium content in the ultrafine section is too low to be identified. Thus, contrast-enhancing approach in HAADF images is directly associated to the thickness of the material that the electron beam passed through. The ultrafine slice of the conidia preparation is about 60nm approximately. In order to identify a nanotube this should be horizontal in the slice which is rarely obtained. The electrodensity found in the lipid vacuoles were identified as osmium, Fig. 7

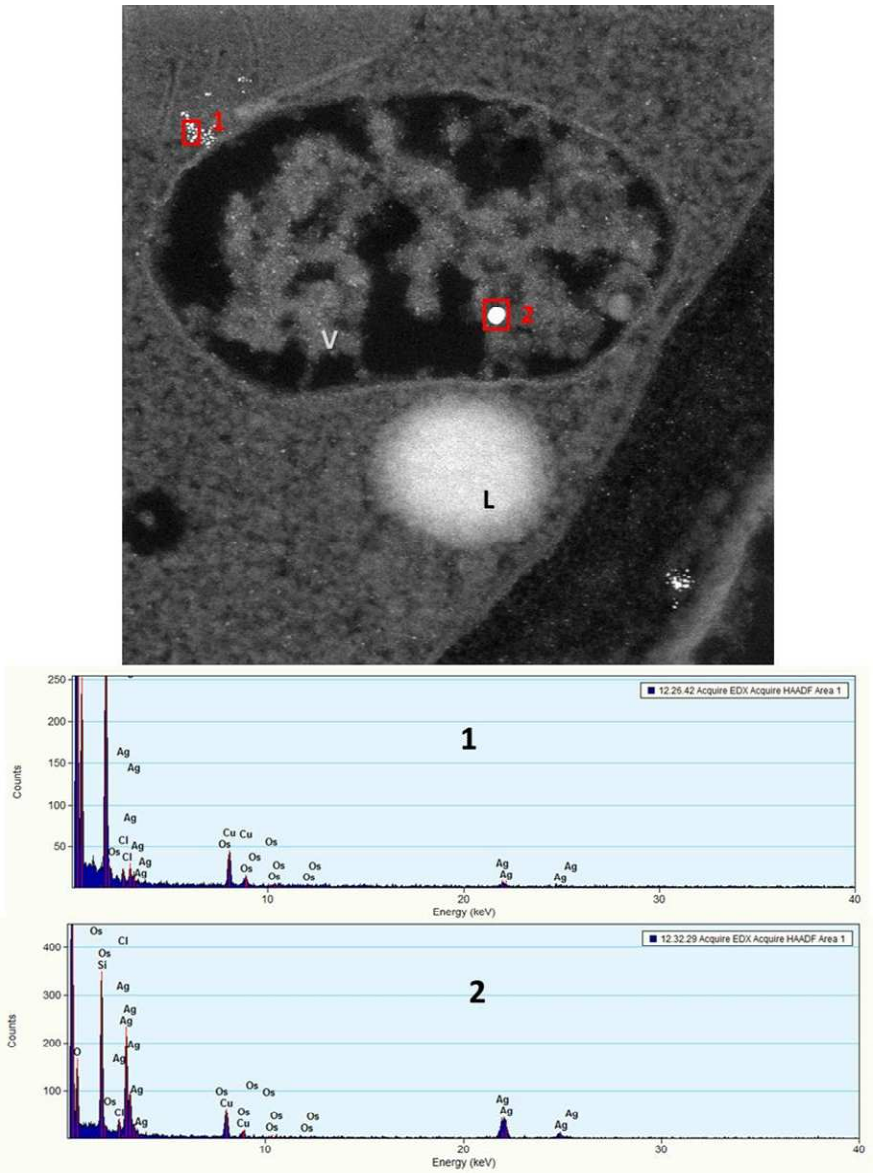

Fig. 7 Selected HAADF images of TNTs0.5Ag photoinactivation, shows Ag dispersed all over the conidia, except on lipid vacuoles and EDS analysis of observed AgNP aggregates.

Thus, the photocatalytic reaction is induced on the silver-titanate surface; the study of surface properties of composites may reveal the interaction way between the photocatalyst and the conidia morphology and structure. In order to allow the characterization and/or quantification of surface reactive species and bactericidal species

(Ag° and AgO), the XPS analysis of the materials was carried out taking into account that titanate materials are layered structures that contains many defects and vacancies and the conditions of the equipment used for obtain XPS spectra.

XPS spectra of O1s and Ti2p for titanate nanotubes and TNT functionalized with 0.5, 1 and 3 wt. % of AgNPs are displayed in Fig. 8a)-h). The O1s spectrum for titanate nanotubes can be deconvoluted by three Gaussian components at 531, 533 and 535 eV and four Gaussian components at 529, 531.5, 533 and 535 eV for TNT functionalized with 0.5, 1 and 3 wt. % of AgNPs. The binding energy at 531 eV can be assigned to oxygen bound to Ti^{4+} ions, likewise binding energy locating at 533 eV can be attributed to oxygen deficiencies and the shoulder located at 532.9 eV implies that the surface is partially covered with hydroxide OH groups. Finally the small shoulder located at 529 can be assigned to silver bound to Ti^{4+}.[14-16] Based on deconvolution analysis the percentage of O^{2-} decreases from 75 to 58 % as the AgNP loading increases. This means that silver nanoparticle functionalization occupies some oxygen surface vacancies, Table 2. The Ag 3d spectra are shown in Fig. 9a-c, the Ag $3d_{5/2}$ and Ag $3d_{3/2}$ peaks were found at the binding energies of 369 eV and 375 eV, respectively. Additionally, the interval of the 3d doublet of Ag is 6.0 eV. The binding energy of Ag $3d_{5/2}$ core level for TNT functionalized with 1 and 3 wt of AgNPs was deconvoluted into three Gaussian components using Shirley background, where Ag^0 and Ag^{+1} are located at 368 and 369.1 , respectively.[38-40] At one with the deconvolution analysis, we found that 65% and 40 % correspond to silver Ag^0 metallic state whereas 60% and 35 % correspond to silver atoms Ag^+ for TNT functionalized with 1 and 3 %wt., respectively. This clearly shows the increase in intensity of $Ag_{5/2}$ and $Ag_{3/2}$ peaks as a function of the silver loading, which are the deconvoluted spectra for composites with 1 and 3% of silver.

The binding energies for Ti $2p_{3/2}$ and $2p_{1/2}$ were displayed at 460 and 465.7 eV and showed the distance of 5.7eV, see in Fig. 8e-h, which is the typical spectra of Ti^{4+} in TiO_2.[41-42] However, the deconvolution display trace of Ti^{3+} was found in titanate nanotubes and TNT functionalized with 0.5, 1 and 3 wt, with 10, 30, 22 and 21 %, respectively. The $H_2Ti_3O_7.H_2O$ phase, normally is attributed to the negatively charged 2-D TiO_6 containing layers separated by interlayer distances (normally from 0.7 to 0.8 nm), is due to exchangeable cations and molecules found in the interlayer cavities or water.[20] Intrinsic $H_2Ti_3O_7.H_2O$ defects such as Ti^{3+} species and oxygen vacancies are observed in the deconvoluted spectra, where an increase in Ti^{3+} defects appears with silver functionalization due to the distorted surface titanate framework, see Fig. 8. The Ag-O bond is observed, probably being due to the interface with titanate surface. Instantaneous assisted photoexcitation of Ag electrons to higher energy states are probably occurring to enhance *B. cinerea* inactivation. In the case of *E. coli,* electron acceptors, and the electrons generated from the Ag nanoparticles due to the small SPR surface are helpful for photokilling the bacteria.[43-44]

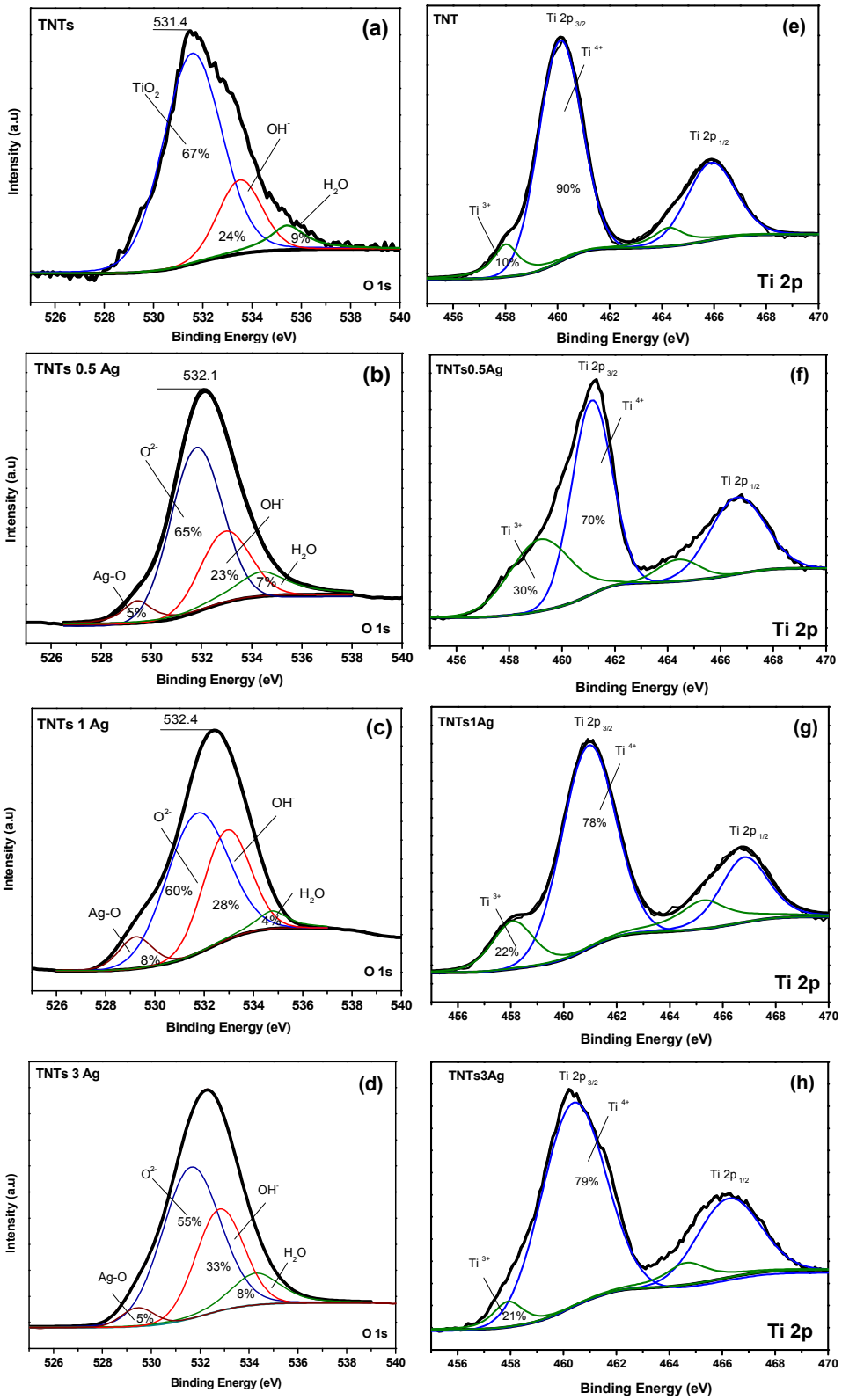

Fig.8. O1s and T12p deconvoluted spectra for TNTs functionalized with different silver loads and TNTs.

Direct contact between the pathogenic fungus and semiconductor powders is necessary to induce fatal damages to the conidium body, where the semiconductor surrounds and covers the conidia. After 7 min, the conidium body is deformed and starts to expand the vacuole up to its physical limit.[11-12] The role of the silver particles consists in capturing electrons and enhancing the electron separation due to the Schottky barrier.[45] In addition, the biocide properties of silver inhibit the fungus growth and reproduction. It is likely that silver species form some complexes with galactomannans and glycoproteins that inhibit the fungus reproduction.[46] The photokilling effects are enhanced by the nanotube penetration that allows cell membrane permeation, which accelerates the vacuole voiding.

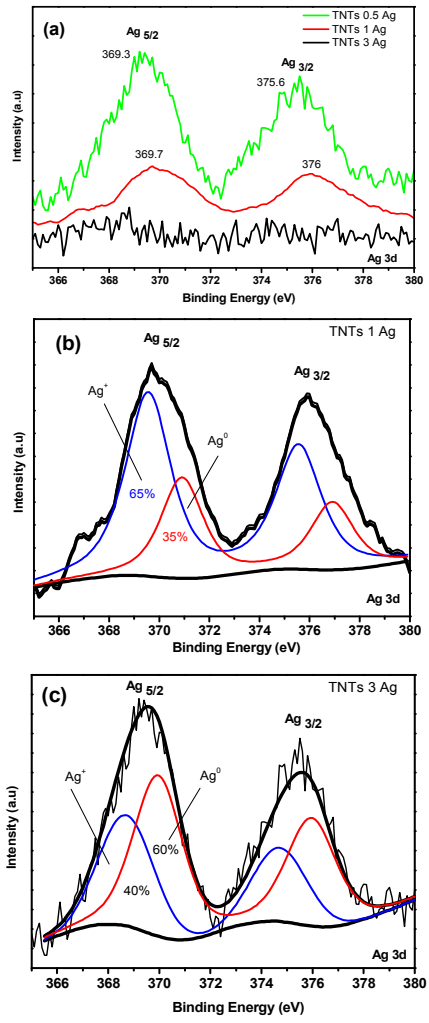

Fig.9. a) Comparative Ag 3d spectra for TNTs functionalized with different silver loads, and b) Ag 3d deconvoluted spectra for TNTs functionalized with 1 and c) 3 wt. % of silver loading

XPS and EDS values are punctual techniques, it depends of the zone analyzed, instead an inductively coupled plasma optical emission spectroscopy (ICP-OES) using a 730-ES spectrometer from Varian Inc analysis was carried out in the samples in order to determinate the real load of AgNPs in each catalyst and this is reported in table 2. The results confirm the stability of the materials.

Table 2: ICP loading of silver and XPS ratios of silver and oxygen as a function of titanio.

Catalyst	Ag content (ICP-OES)	Ag/Ti Ratio by XPS	O/Ti Ratio by XPS
TNTs	0	0	1.8
TNTs 0.5 Ag	0.45	0.005	2.4
TNTs 1 Ag	0.92	0.012	2.6
TNTs 3 Ag	2.45	0.032	3.1

Both light-irradiation and photochemical interruptions result in growth suppression. As it was pointed out by Yi Tao et al.[46] *Microcystis aeruginosa* under UV-C stress is recoverable within 3 days with post-UV incubation. The size of 5nm in average of AgNPs is also a crucial factor of successful inactivation as stated by Morones et al.[47] Only Ag or CuNPs below 10nm present lethal bactericidal properties to gram-negative bacteria.[48] It was demonstrated that surface modification with silver nanoparticles leads to enhanced photoactivity under halogen irradiation, and this effect depends on the amount of loaded AgNPs and the microorganism. Loading a 3% of AgNPs results beneficial to kill *E. Coli*, nonetheless, with only 0.5% of AgNP loading, *B. cinerea* was effectively inactivated.

The difference regarding the inactivation time between *E. Coli* and *B. Cinerea* is closely related to specific interactions with cell wall components and their thickness. It was reported that TiO_2-based materials present a high affinity for phospho-proteins and phospho-peptides in gram-negative bacteria as *E. Coli*.[13,17, 21] The phosphorylation of proteins plays a role in the regulation of cell damage, then the photocatalytic environment causes cell lysis.[15] A further biological approach will be helpful for full understanding of the difference between the pathogenic microorganisms that permit the tailoring of the design of highly active nanomaterials for a specific pathogenic agent.

To verify the Ag content and quantify the silver lixiviation in the titanate nanotubes, inductively coupled plasma optical emission spectroscopy (ICP-OES) using a 730-ES spectrometer from Varian Inc was used. It was detected 1.27 ppm of silver after 1 h of sonication 50 mg of TNTsAg3 in 50 mL of deionized water and 21.8 ppm in the case of Ti.

Nanotubular nanostructures have been one of the most important research subjects in the design of nanomaterials. The most known are the multi-walled carbon nanotubes MWCNT that possess a detrimental toxicity due to the composition and method of synthesis. MWCNTs are an allotrope of sp^2 hybridized carbon having great chemical stability. However, it is necessary to functionalize the nanotubes to enhance both the strength and water dispersibility of composites. The MWCNT with 15 nm can inactivate pathogenic elements when their cell wall is conjugated with a degrading enzyme. A laborious PEG-based link between the nanotube and enzyme resulted in enhanced bactericidal activity for staphylococci, including methicillin-resistant strains of *S. aureus*.[49] However, MWCNT are still expensive and toxic for human or food applications,

which is in contrast with our proposal of ultrathin silver titanate nanotubes as eco-friendly nanocomposite antifungal materials. This nanostructure provides a material that is not toxic and supports both photoactivity at room temperature and bactericidal catalysis. This fact demonstrates the breadth of natural antimicrobial catalysts for a gram-negative pathogenic bacteria and phytopahtogenic fungus.

Inactivation consists not only of the AgNP biocidal effect but also of the photogeneration of radical oxygen species that injure the cell wall.[14, 17] On the other hand, the coordination of silver with the content of vacuoles and plasmalemma produces vacuolation and invaginations that gradually kill the cells in maximum 30 min. The synergic effect inhibits the germination and growth of mycelium,[13-14] which makes this photoinactivation process irreversible. The impact of eco-friendly inactivation is significant because of the ease to carry out the inactivation that may possibly be performed *in-situ* over plants like tomato or grapes, using impregnation on transparent fibers with the nanomaterials or in a composite film with a translucent biopolymer in order to be activated with natural sun radiation.

Conclusions

To the best of our knowledge, this is the first time that titanate silver nanocomposites reached the rapid inactivation of the phytopathogenic fungus *Botrytis cinerea* in 20 minutes.

The preparation of silver–titanate semiconductors by the hydrothermal method assisted by microwave irradiation allows the rapid formation of nanocomposites with central

properties that induce the following irreversible effects on the *B. cinerea* fungus: (i) high dispersion of AgNP species, AgO, and Ag°, all over de titanate nanotubes enhances the charge separation for generating ROS species that stress the fungus, (ii) boosts the biocide effect on the *B. cinerea* conidia, which inhibits its propagation, and (iii) the nanotube morphology damages the cell wall, accelerating the vacuolation and invaginations that produce fatal inactivation of the pathogenic fungus.

The unusual synergetic properties of the silver/titanate nanomaterials, their low cost and practical synthesis show that these composites are promising green materials that can successfully photokill pathogenic fungi such as *B. cinerea* within minutes.

Acknowledgements

The authors want to thank N. Angelica Ramírez Pérez and N. Gómez Hernández for their technical help during the inactivation experiments. We gratefully acknowledge G. Labrada Delgado and H. Silva Pereyra from LINAN-IPICYT for the FESEM and HRTEM material characterizations. This work was supported by Infra-2014/225945 and CB-2013/220791 CONACyT projects. R.B. D-E thanks CONACyT for the Ph.D. scholarship. The research of this paper was supported by the he MSIP (Ministry of Science, Ict & future Planning).

References

(1) Waller, J.M.; Lenné, J.M; Waller, S.J. (Eds). Plant Pathologist´s Pocketbook. *CABI Publishing.* **2002,** 3rd edn, 1-487.

(2) Elad, Y.; Williamson, B.P.; Tudzynski, P.; Denle, N. *(Eds).* Botrytis: Biology, *Pathology and Control.* Springer Netherlands. **2007,** 1st edn, 1-254.

(3) Divon, H.; Fluhr, H.R. Nutrition Acquisition Strategies During Fungal Infection of Plants. FEMS *Microbiol Lett.* **2007**, 266, 65-74.

(4) González-Collado, I.; Macías-Sánchez, A.J.; Hanson, J.R. Fungal Terpene Metabolites: Biosynthetic Relationships and the Control of the Phytopathogenic Fungus Botrytis *cinerea. Nat. Prod. Rep.* **2007**, 24, 674-686.

(5) Huang, S.; Wang, L.; Liu, L.; Hou, Y.; Li, L. Nanotechnology in Agriculture, Livestock, and Aquaculture in China. A review. *Agron. Sustain. Dev.* **2015**, 35, 369-400.

(6) Clarkson, J.; Whipps, J. Control of Sclerotial Pathogens in Horticulture. *Pestic. Outlook.* **2002,** 13, 97-101.

(7) Myung, K.; Hamilton-Kemp, T.R.; Archbold, D.D. Interaction with and Effects on the Profile of Proteins of *Botrytis cinerea* by C6 Aldehydes. *J. Agric Food Chem.* **2007**, 55, 2182-2188.

(8) Liu, J.L.; Luo, Z.; Bashir, S.A. Progressive Approach on Inactivation of Bacteria Using Silver-Titania Nanoparticles. *Biomater. Sci* **2013**, 1, 194-201

(9) Villa-Rojas, R.; Sosa-Morales, M.E.; Lopez-Malo, A.; Tang, J. Thermal Inactivation of *Botrytis cinerea* Conidia in Synthetic Medium and Strawberry Puree. *Int J. Food Microbiol.* **2012**, 155, 269-272.

(10) Ou, H.; Gao, N.; Deng, Y.; Qiao, J.; Zhang, K.; Li, T.; Dong, L. Mechanistic Studies of Microcystic Aeruginosa Inactivation and Degradation by UV-C Irradiation and Chlorination with Poly-Synchronous Analyses. *Desalination.* **2011**; 272, 107-119.

(11) Li, Q.; Ning, P.; Zheng, L.; Huana, J.; Li, G.; Hsiang, T. Effects of Volatile Substances of Streptomyces Globisporus JK-1 on Control of *Botrytis cinerea* on Tomato Fruit. *Biol. Control.* **2012**, 61, 113-120.

(12) He, L.; Liu, Y.; Mustapha, A.; Lin, M. Antifungal Activity of Zinc Oxide Nanoparticles Against *Botrytis cinerea* and *Penicillium Expansum*. *Microbiol. Res.* **2011**, 166, 207-215.

(13) Kubacka, A.; Suárez Diez, M.; Rojo, D.; Bargiela, R.; Ciordia, S.; Zapico, I.; Albar, J. P.; Barbas, C.; Martins dos Santos, V. A. P.; Fernández-García, M.; Ferrer, M. Understanding the Antimicrobial Mechanism of TiO_2-based Nanocomposite Films in a Pathogenic Bacterium. *Sci. Rep.* **2014**, 4, 4134.

(14) Rodríguez-González, V.; Obregón-Alfaro, S.; Torres- Martínez, L. M.; Cho, S-H.; Lee, S-W. Silver-TiO_2 Nanocomposites: Synthesis and Harmful Algae Bloom UV Photoelimination. *Appl. Catal. B-Environ.* **2010**, 98, 229-234.

(15) Thabet, S.; Simonet, F.; Lemaire, M.; Guillard, C.; Cotton, P. Impact of Photocatalysis on Fungal Cells: Depiction of Cellular and Molecular Effects on *Saccharomyces cerevisiae*. *Appl. Environ. Microb.* **2014**, 80, 7527-7535.

(16) Hossain F.; Perales-Perez, O.J.; Hwang S.; Román F., Antimicrobial Nanomaterials as Water Disinfectant: Applications, Limitations and Future Perspectives. *Sci. Total Environ.* **2014**, 466-467, 1047-1059.

(17) Foster, H.A.; Ditta, I.B.; Varghese, S.; Steele, A. Photocatalytic Disinfection Using Titanium Dioxide: Spectrum and Mechanism of Antimicrobial Activity. *Appl. Microbiol. Biot.* **2011**, 90, 1847-1868.

(18) Zhang J.; Liu Y.; Li Q.; Zhang X.; Shang J.K. Antifungal Activity and Mechanism of Palladium-Modified Nitrogen-Doped Titanium Oxide Photocatalyst on Agricultural Pathogenic Fungi Fusarium graminearum. *ACS Appl. Mater. Interfaces.* **2013**, 5, 10953−10959

(19) Lui N.; Chen X.; Zhang J.; Schwank J.W., A Review on TiO_2-Based Nanotubes Synthesized Via Hydrothermal Method: Formation Mechanism, Structure Modification, and Photocatalytic Applications. *Catal. Today.* **2014**, 225**,** 34-51

(20) Zhang Y.; Jiang Z.; Huang J.; Lim L.Y.; Li W.; Deng J.; Gong D.; Tang Y.; Lai Y.; Chen Z. Titanate and Titania Nanostructured Materials for Environmental and Energy Applications: a Review. *RSC Advances.* **2015**, 5, 79479-79510.

(21) Guzman, M.; Dille, J.; Godet, S. Synthesis and Antibacterial Activity of Silver Nanoparticles Against Gram-Positive and Gram-Negative Bacteria. *Nanomed-Nanotechnol.* **2012**, 8, 37-45.

(22) Rodríguez-González, V.; Obregón-Alfaro, S.; Lozano- Sánchez, L. M.; Lee, S-W. Rapid Microwave-Assisted Synthesis of One-Dimensional Silver-$H_2Ti_3O_7$ Nanotubes. *J. Mol. Catal A- Chem.* **2012**, 353-354, 163-170.

(23) Salas-Marina, M. A.; Silva-Flores, M. A.; Uresti-Rivera, E. E.; Castro-Longoria, E.; Herrera-Estrella, A.; Casas-Flores. S. Colonization of Arabidopsis roots by Trichoderma

atroviride Promotes Growth and Enhances Systemic Disease Resistance through Jasmonate and Salicylate Pathways. Eur. J. Plant Pathol. **2011**, 131, 15-26.

(24) Xiong, Z.; Ma, J. Ng, W.J.; Waite, T.D.; Zhao, X.S. Silver-Modified Mesoporous TiO_2 Photocatalyst for Water Purification. *Water Res.* **2011**, 45, 2095-2103.

(25) Alrousan, D.M.; Dunlop, P.S.M.; McMurray, T.A.; Byrne, J.A. Photocatalytic Inactivation of *E. coli* in Surface Water Using Immobilised Nanoparticle TiO_2 Films *Water Res.* **2009**, 43, 47-54.

(26) Giridhar, M.; Modak, J.M.; Sontakke, S. Photocatalytic Inactivation of *E. coli* and *Pichia pastoris* with Combustion Synthesized Titanium Dioxide. *Chem. Eng. J.* **2010**, 165, 225-233.

(27) Ou, H-H.; Lo, S-L. Review of Titania Nanotubes Synthesized via the Hydrothermal Treatment: Fabrication, Modification, and Application. *Sep. Purif. Technol.* **2007**, 58, 179-191.

(28) Roth, W.J.; Gil, B.; Makowski W.; Marszaleka B.; Eliasova P., Layer Like Porous Materials with Hierarchical Structure. Chem. Soc. Rev. **2016**, 45, 3400-3438.

(29) Zhang, M.; Jin, Z.; Zhang, J.; Guo, X.; Yang, J.; Li, W.; Wang, X.; Zhang, Z. Effect of Annealing Temperature on Morphology, Structure and Photocatalytic Behavior of Nanotubed $H_2Ti_2O_4(OH)_2$. *J. Mol. Catal A- Chem.* **2004**, 217, 203-210.

(30) Khazaeli, P.; Zamanizadeh, H.; Morid, B.; Bayat, H. Morphological and Molecular Identification of *Botrytis Cinerea* Causal Agent of Gray Mold in Rose Greenhouses in Centeral Regions of Iran. *IJASR*. **2010**, 1, 19-24.

(31) Hawker, L.E.; Hendy, R.J. An Electron-Microscope Study of Germination of Conidia of *Botrytis cinerea*. *J. Gen. Microbiol*. **1963**, 33, 43-46.

(32) Buckley, P.M.; Sjaholm, V.E.; Sommer, N.F. Electron Microscopy of *Botrytis cinerea* Conidia. *J. Bacteriol* **1966**, 91, 2037-2044.

(33) Leroch, M.; Kleber, A.; Silva, E.; Coenen, T.; Koppenhöfer, D.; Shmaryahu, A.; Valenzuela, P.D.T.; Hahn, M. Transcriptome Profiling of *Botrytis cinerea* Conidial Germination Reveals Upregulation of Infection-Related Genes During the Prepenetration stage. *Eukaryot Cell.* **2013**, 12, 614-626.

(34) Elvio Amato, E.; Diaz-Fernandez, Y.A.; Taglietti, A.; Pallavicini, P.; Pasotti, L.; Cucca, L.; Milanese, C.; Grisoli, P.; Dacarro, C.; Fernandez-Hechavarria, J.M.; Necchi, V.

Synthesis, Characterization and Antibacterial Activity Against Gram Positive and Gram Negative Bacteria of Biomimetically Coated Silver Nanoparticles. *Langmuir.* **2011**, 27 (15), 9165–9173.

(35) Reddy, B.M.; Sreekanth, P.M.; Reddy, E.P.; Yamada, Y.; Xu, Q.; Sakura, H.; and Kobayashi, T. Surface Characterization of La_2O_3−TiO_2 and V_2O_5/La_2O_3−TiO_2 Catalysts, *J. Phys. Chem. B.* **2002**, 106, 5695-5700.

(36) Xin, B.; Jing, L.; Ren, Z.F.; Wang, B.; and Fu, H. Effects of Simultaneously Doped and Deposited Ag on the Photocatalytic Activity and Surface States of TiO_2, *J. Phys. Chem. B.* **2005,** 109, 2805-2809.

(37) Sanjinés, R.; Tang, H.; Berger, H.; Gozzo, F.; Margaritondo, G.; and Levy, F. Electronic Structure of Anatase TiO_2 Oxide**,** *J. Appl. Phys.* **1994**, 75, 2945-2951.

(38) Martinez-Castanon, G.A.; Nino-Martinez, N.; Martinez-Gutierrez, F.; Martinez-Mendoza, J.R.; and Ruiz, F. Synthesis and Antibacterial Activity of Silver Nanoparticles with Different Sizes, *J. Nanopart. Res.* **2008**, 10, 1343–1348.

(39) Liang, Y.Q.; Cui, Z.D.; Zhu, S.L.; Liu, Y.; Yang. X.J. Silver Nanoparticles Supported on TiO_2 Nanotubes as Active Catalysts for Ethanol Oxidation, *J. Catal.* **2011**, 278, 276–287.

(40) Moulder, J.F.; Stickle, W.F.; Sobol, P.E.; and Bomben, K.D.; Handbook of X-ray Photoelectron Spectroscopy, Perking-Elmer Corp., Physical Electronics Division, *Eden Prairie*, MN, **1992**.

(41) Wang, S.; Qian, H.; Hu, Y.; Dai, W.; Zhong, Y.; Chen, J.; and Hu, X. Facile One-Pot Synthesis of Uniform TiO_2–Ag Hybrid Hollow Spheres with Enhanced Photocatalytic Activity, *Dalton Trans.* **2013**, 42**,** 1122–1128.

(42) Su, C.; Liu, L.; Zhang, M.; Zhang. Y.; and Shao, C. Fabrication of Ag/TiO_2 Nanoheterostructures with Visible Light Photocatalytic Function via a Solvothermal Approach, *Cryst. Eng. Commun.* **2012**, 14**,** 3989–99.

(43) Linic, S.; Christopher, P.; Ingram, D.B. Plasmonic-metal Nanostructures for Efficient Conversion of Solar to Chemical Energy. *Nature Materials.* **2011**, 10, 911-921.

(44) Albersheim, P.; Darvill, A.; Roberts, K.; Sederoff, R.; Staehelin, A. Plant Cell Walls 1st Edition, Garland Science *Taylor & Francis* Group, **2011**.

(45) Devi, L.G.; Kavitha, R. A Review on Plasmonic Metal–TiO_2 Composite for Generation, Trapping, Storing and Dynamic Vectorial Transfer of Photogenerated Electrons Across the Schottky Junction in a Photocatalytic System. *Appl. Surf. Sci.* **2016**, 360 part B, 601-622.

(46) Tao, Y.; Zhang X.; Au, D. W.T.; Mao, X.; Yuan, K. The Effects of Sub-Lethal UV-C Irradiation on Growth and Cell Integrity of Cyanobacteria and Green Algae. *Chemosphere.* **2010**, 78, 541-547.

(47) Morones, J.R.; Elechiguerra, J.L.; Camacho, A.; Holt, K.; Kouri, J.B.; Ramírez, J.T.; Yacaman, M.J. The Bactericidal Effect of Silver Nanoparticles. *Nanotechnology.* **2005**, 16, 2346-2353.

(48) Cindy Gunawan, C.; Wey Yang Teoh, W.Y.; Marquis, C.P.; Amal, R., Cytotoxic Origin of Copper (II) Oxide Nanoparticles: Comparative Studies with Micron-Sized Particles, Leachate, and Metal Salts. *ACS Nano.* **2011**, 9, 7214–7225

(49) Pangule, R.C.; Brooks, S.J.; Dinu, C.Z.; Bale, S.S.; Salmon, S.L.; Zhu, G.; Metzger, D.W; Kane R.S.; Dordick J.S. Antistaphylococcal Nanocomposite Films Based on Enzyme−Nanotube Conjugates, *ACS Nano.* **2010**, 4 (7), 3993–4000.

Antifungal Nanocomposites Inspired by Titanate Nanotubes for Complete Inactivation of *Botrytis cinerea* Isolated from Tomato Infection.

V. Rodríguez-González,[1] R. B. Domínguez-Espíndola,[2] S. Casas-Flores,[3] O. A. Patrón-Soberano[3], R. Camposeco-Solis[1] and S-W. Lee[4]*

*Corresponding Author: V. Rodríguez-González, Ph.D.

E-mail: vicente.rdz@ipicyt.edu.mx

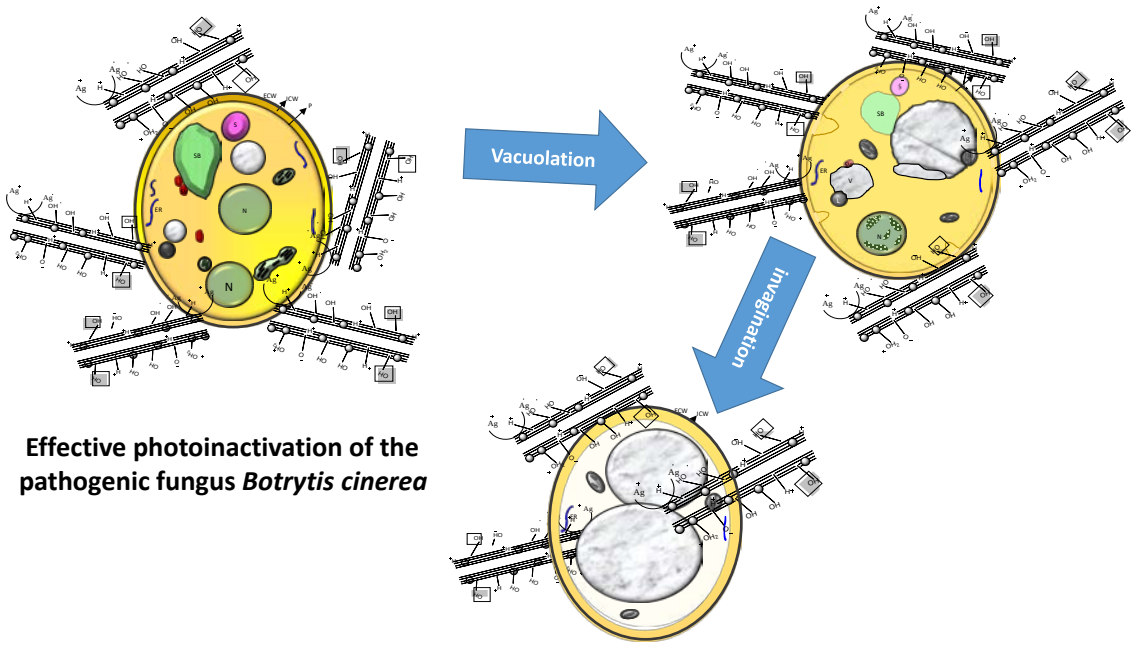

Effective photoinactivation of the pathogenic fungus *Botrytis cinerea*